Analytical Solution to 3D SPECT Reconstruction with Non-uniform Attenuation, Scatter, and Spatially-variant Resolution Variation for Variable Focal-length Fan-beam Collimators

Junhai Wen*, Hongbing Lu, Tianfang Li, and Zhengrong Liang
Department of Radiology, State University of New York, Stony Brook, NY 11794, USA

ABSTRACT

In the past decades, analytical (non-iterative) methods have been extensively investigated and developed for the reconstruction of three-dimensional (3D) single-photon emission computed tomography (SPECT). However, it becomes possible only recently when the exact analytic non-uniform attenuation reconstruction algorithm was derived. Based on the explicit inversion formula for the attenuated Radon transform discovered by Novikov (2000), we extended the previous researches of inverting the attenuated Radon transform of parallel-beam collimation geometry to fan-beam and variable focal-length fan-beam (VFF) collimators and proposed an efficient, analytical solution to 3D SPECT reconstruction with VFF collimators, which compensates simultaneously for non-uniform attenuation, scatter, and spatially-variant or distance-dependent resolution variation (DDRV), as well as suppression of signal-dependent non-stationary Poisson noise. In this procedure, to avoid the reconstructed images being corrupted by the presence of severe noise, we apply a Karhune-Loève (K-L) domain adaptive Wiener filter, which accurately treats the non-stationary Poisson noise. The scatter is then removed by our scatter estimation method, which is based on the energy spectrum and modified from the triple-energy-window acquisition protocol. For the correction of DDRV, a distance-dependent deconvolution is adapted to provide a solution that realistically characterizes the resolution kernel in a real SPECT system. Finally image is reconstructed using our VFF non-uniform attenuation inversion formula.

Keywords: Analytical reconstruction, non-uniform attenuation, Poisson noise reduction, scatter, distance-dependent resolution variation, attenuated Radon transform, and variable focal length fan-beam geometry.

1. INTRODUCTION

SPECT is a cost-effective functional imaging modality and aims to reconstruct an image of the uptake distribution within the tissues or organs of radiopharmaceutical or radiotracer, which is injected intravenously into the patient. The reconstruction is based on the measurement of radiation emitted by the radiotracer. Because of photoelectric absorption and Compton scattering, the emitted γ photons are attenuated inside the body before arriving at the detector. Meantime, there is always unavoidable detector blurring effect due to the finite size of the collimator holes. The detector response in reality is spatially varying and deteriorates with distance from the face of the collimators. It is called DDRV, which results in shape distortion and non-uniform density variation in the reconstructed image from projection data obtained from a SPECT imaging system. Currently, most SPECT protocols for clinical application only support quantitative reconstruction. For more accurate diagnosis, quantitative reconstruction of radiotracer concentration at any location inside the body is desired and requires accurate compensation for the attenuation, scatter, and DDRV, as well as accurate treatment of the Poisson noise.

Currently available analytical method is the filtered backprojection (FBP) method, which is considerably faster and widely used in clinic. Analyzing the noise property of its reconstruction is straightforward. But it is very challenging to derive an explicit inversion formula based on the realistic mathematical models of the SPECT measurements within the FBP framework. In the past decades, a great research effort has been devoted to investigate and develop various analytical means that can simultaneously correct for uniform attenuation and DDRV for quantitative 3D SPECT reconstruction [4][6][11][14][29]. The correction for non-uniform attenuation becomes possible only recently when the exact analytic non-uniform attenuation reconstruction algorithm was derived by Novikov [19] in year

* wenjh@clio.mil.sunysb.edu; phone 1 631-444-7999; fax 1 631-444-6450. This work was supported in part by a NIH Grant #HL51466.

Medical Imaging 2003: Image Processing, Milan Sonka, J. Michael Fitzpatrick, Editors,
Proceedings of SPIE Vol. 5032 (2003) © 2003 SPIE · 1605-7422/03/$15.00

2000. In his paper, Novikov presented an explicit formula for inverting the attenuated Radon transform for SPECT reconstruction with parallel-beam collimator geometry. Natterer [18] reported another version of the formula later. These formulas had been implemented and good reconstruction results were obtained [10]. Based on the explicit inversion formula for the non-uniform attenuated Radon transform, we further developed an efficient, analytical solution to 3D quantitative SPECT reconstruction of parallel-beam collimator geometry with simultaneous compensation for attenuation, scatter, and DDRV, as well as accurate treatment of Poisson noise [17].

For many clinical applications, however, fan-beam and VFF collimation geometries are preferred. Fan-beam collimator improves count density and spatial resolution, as compared to parallel-beam collimator, for imaging small objects, such as small animals and the human head with distorted skull enclosure. (A normal skull enclosure can be treated as a thickened brain tissue shell and therefore the attenuated Radon transform reduces to the exponential Radon transform). For cardiac studies, however, the fan-beam geometry encounters truncation problem, due to its limited acceptance angle across the field-of-view (FOV), which can cause artifacts. The VFF collimator overcomes this truncation problem, while preserving the improved count density and spatial resolution. In our previous work, based on the parallel-beam non-uniform attenuation inversion formula of Novikov and the relation between the parallel-beam geometry and variable fan-beam geometry, we derived our variable fan-beam non-uniform attenuation inversion formula [25][26][27]. Meantime, we investigated the frequency-distance relation (FDR) in fan-beam and variable fan-beam geometries and studied the frequency to trajectory relation in these non-parallel geometries. Based on these investigations, we constructed a non-stationary FDR filter with reasonable approximation to compensate for the detector blurring effect of the fan-beam and variable fan-beam geometries [12]. Accurate treatment of the DDRV is under progress [13].

It is true for all inverse solutions that analytical reconstruction methods that compensate for the attenuation-resolution effects can be highly susceptible to data noise and model errors. To avoid reconstructed images being corrupted by the presence of severe noise and conspicuous artifacts, we first apply our K-L domain adaptive Wiener filter, which accurately treats the signal-dependent Poisson noise in the primary and scatter window measurements. The scatter contribution to the primary-energy-window measurements is then removed by our scatter estimation method, which is based on the energy spectrum and modified from the triple-energy-window acquisition protocol.

Based on the above previous researches, we build in this paper an analytical framework for the solution of 3D quantitative SPECT reconstruction with VFF collimators, which provides a simultaneous compensation for non-uniform attenuation, object-specific scatter, and spatially variant resolution variation, as well as an accurate treatment of the non-stationary Poisson noise.

2. RECONSTRUCTION SCHEME

In general, the sinogram in 3D SPECT with non-uniform attenuation, DDRV, scatter and noise can be expressed as

$$g_\phi(p,q) = \iiint f(x,y,z)h(x,y,z,\phi,p,q)e^{-\int a(x',y',z')dl}dxdydz + r(\phi,p,q) + n(\phi,p,q) \qquad (1)$$

where $a(x,y,z)$ is the attenuation coefficient map of the body, $h(x,y,z,\phi,p,q)$ is the DDRV function of the SPECT system, $f(x,y,z)$ is the radiotracer activity distribution inside the body, $r(\phi,p,q)$ denotes the background events such as scatter contribution, and $n(\phi,p,q)$ is the noise.

With the existence of random noise and other deterministic physics effects, we propose an analytical reconstruction scheme that corrects simultaneously for all the above degrading factors, as shown in Figure 1. In the following subsections, we will describe our analytical reconstruction scheme in details.

2.1 K-L Domain Adaptive Wiener Filtering for Accurate Treatment of Poisson Noise

As is true for all inverse solutions, analytical reconstruction methods that compensate for the attenuation can be highly susceptible to data noise and model errors. Therefore, these methods should be regularized adequately so that they are numerically robust and can yield quantitatively accurate images. To avoid reconstructed images being corrupted by the presence of severe noise and conspicuous artifacts, we first apply our K-L domain adaptive Wiener

filter, which accurately treats the signal-dependent Poisson noise in the primary and scatter window measurements. The task of spatial filtering of signal-dependent Poisson noise can be greatly simplified by first applying the Anscombe transform to all the projection data, which converts Poisson distributed noise into Gaussian distributed one with a constant variance [1]. That is, if x is Poisson distributed with mean equal to λ, then $y=(x+3/8)^{1/2}$ can be approximated as Gaussian distributed with mean equal to $(\lambda+1/8)^{1/2}$ and variance of 0.25. Therefore, by Anscombe transformation, the noise becomes signal independent and can be expressed mathematically as an additive term. In this situation, the noise covariance matrix of the transformed projection data is the identity matrix (with unit variance and being uncorrelated) being multiplied by 0.25.

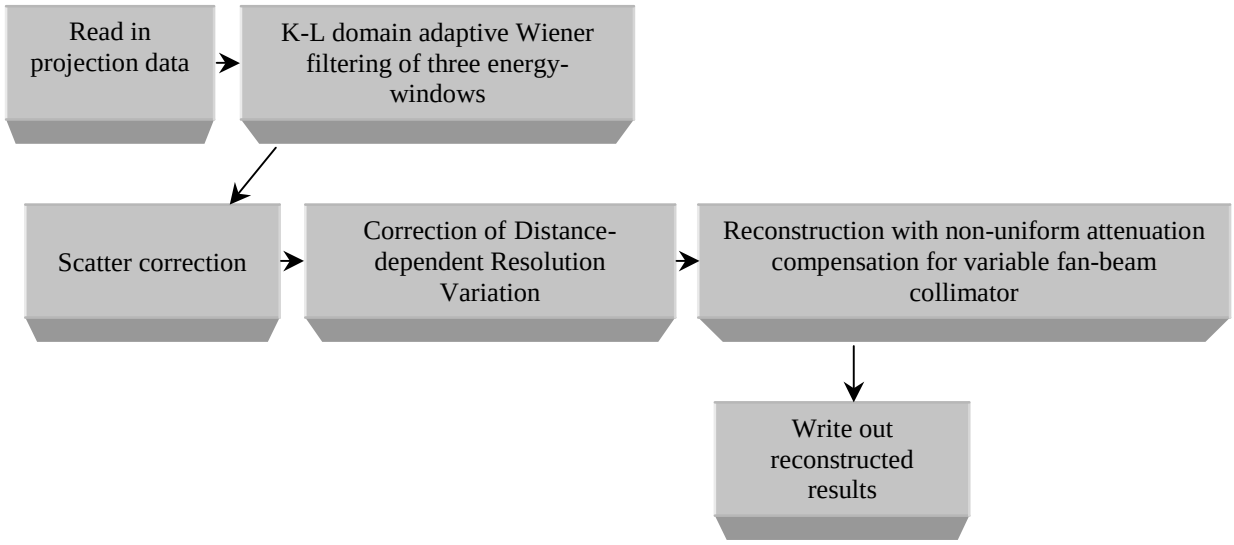

Figure 1: Flow chart for proposed reconstruction scheme.

It has been proved that in the K-L domain, the noise property of constant variance remains for all components [16]. By applying K-L transform on equation (1), we have

$$W = A_M g = A_M g' + A_M n' = g_l + n_l \tag{2}$$

where $A_M = A \otimes I_M$ and A is a $K \times K$ matrix composed of eigenvectors of the covariance matrix K_t between different sinograms. Notation I_M denotes an $M \times M$ identity matrix and $\otimes$ represents the Kronecker product.

The Wiener restoration in the K-L domain can be expressed by K independent filters each for one principal component [16][9]:

$$g_{li} = d_i K_s (d_i K_s + \sigma_n^2 I_M)^{-1} W_i, \quad i = 1,2,...,K \tag{3}$$

where K_s is the spatial covariance within the sinograms, d_i is the i-th eigenvalue of the covariance matrix K_t, and σ_n^2 is a constant equal to 0.25. If spatial stationarity for each principal component is utilized, the 2D wiener filter in the K-L domain is the expressed as

$$H(\omega_s, k_\theta) = \frac{S_{g_i}(\omega_s, k_\theta) - \sigma_n^2}{S_{g_i}(\omega_s, k_\theta) + (\beta - 1)\sigma_n^2} \tag{4}$$

where S_{g_i} is the 2D discrete Fourier transform (FT) of sinogram g_i for image slice i, (ω_s, k_θ) demotes the 2D FT coordinates, and β is a smoothing parameter, controlling the degree of smoothness and usually equal to 1 for SPECT study. The K-L domain Wiener filtering is the product of equations (3) and (4) in the FT space.

2.2 Scatter Correction Based on a Triple-Energy-Window Acquisition Strategy

After suppression of Poisson noise, the scatter contribution to the primary-energy-window is then removed by our scatter estimation method [13], which is based on the detection energy spectrum and modified from the triple-energy-window acquisition protocol [20]. In our triple energy window strategy, we select the main window (W_m: 128 keV-152 keV) centered at the peak energy of 140 keV, and the two satellite windows (W_l and W_u with 4 keV width) centered at 126 keV and 154 keV respectively. The scattered photon counts within the main window are described as the following equation:

$$C_{sca} = \frac{2}{3}\left(\frac{C_l}{W_l} - x\frac{C_u}{W_u}\right)W_m \tag{5}$$

where x is the ratio between C_l/W_l and C_u/W_u in the absence of attenuation and scatter, which removes the assumption that the primary photons inside both the satellite windows are the same. The value of x is determined by measuring a point source in air. When x value is equal to 1, our method is reduced to the Bourguignon's method [3]. The scatter energy spectrum inside the photo-peak or main window is closely represented by a parabola function, rather than a linear function as assumed in both Ogawa's and Bourguignon's method [3][20]. The area under the parabola spectrum can be accurately computed through an integral operation, given the heights at 126 keV and 154 keV locations. Therefore, a scale factor 2/3, rather than ½, is shown in our new algorithm. This non-liner scatter energy spectrum within the main window is fundamentally different from both Ogawa's and Bourguignon's methods, in addition to the different treatment of primary photon counts in both satellite windows.

2.3 The Correction of DDRV for VFF collimators

For the correction of DDRV [6][23][29][36][37], we investigated the frequency-distance relation (FDR) in fan-beam and VFF geometries and studied the frequency to trajectory relation in these non-parallel geometries. Based on the investigation we constructed a non-stationary FDR filter with reasonable approximation to compensate for the detector blurring effect of the fan-beam and VFF geometries [12]. Accurate treatment of DDRV is under progress [13].

According to the detector response model of VFF geometry, the blurred projection data can be expressed, under the collimator coordinate system (CCS), as:

$$g^b(\theta,\xi) = \int_{-\infty}^{\infty} d\eta \int_{-\infty}^{\infty} d\xi^* w(\xi^*,\eta) f(\theta,\eta,\xi^*) h(\xi^*,\xi-\xi^*,\eta) \tag{6}$$

where $w(.)$ is the Jacobian factor for VFF and is given by

$$w(\xi,\eta) = 1 - \frac{\eta}{F} + \frac{\eta\xi F'}{F^2} \tag{7}$$

and $h(.)$ is the point spread function (PSF) for the VFF geometry. Notation F is the focal length function and F' is the first-order differentiation.

Note that the collimator-blurred data is no longer a convolution of object with PSF, it also depends on the source position. Generally speaking, the integral of equation (6) cannot be separated to generate the filter as in the parallel-beam collimation case.

A first simple consideration is to use an average PSF $\tilde{h}(.)$ to substitute $h(.)$ in equation (6). After the 2D FT with respect to θ and ξ, it can be shown that

$$g(n,\omega) = g^b(n,\omega)\tilde{H}^{-1}(n,\omega) \tag{8}$$

where $\tilde{H}$ is

$$\tilde{H}(n,\omega) = \int_{-\infty}^{\infty} e^{-2\pi i\omega u}\tilde{h}(u,\eta(n,\omega,\overline{\xi'}))du \tag{9}$$

and $\eta(.)$ stands for the FDR of VFF:

$$\eta = \frac{nF^2 - \omega F(FR_O + \xi^2)}{n(F - F'\xi) - \omega(F^2 + \xi^2)} = \eta(n, \omega, \xi) \tag{10}$$

where R_o is the radius of scan orbit.

Secondly, to better estimate $\tilde{h}(.)$, we note that the PSF is often a sharp function, i.e., only none-zero in a small region, and in this region, we can assume that the PSF does not change much. Therefore, equation (6) can be integrated in segments with $h = h_i(\xi - \xi', \eta)$ in each segment. With this approximation, we chose the average PSF $\tilde{h}(.)$ as $\tilde{h} = \sum_i h_i(\xi - \xi')$.

Usually, resolution enhancement by inverse *H*(.) will have a cost of noise increase. To control the noise in the process, a regularization approach is used via a Wiener filter, which can be expressed as

$$W_F(n, \omega) = \frac{|H(n, \omega)|}{|H(n, \omega)|^2 + \frac{N}{S}} \tag{11}$$

where *N* is the expected value of the power spectrum of the noise process, and *S* is an estimate of the power spectrum of the random process of which the object is assumed to be a sample.

The formulas above are in 2D space, but it is easy to extend them to 3D space. The formulas were implemented in three dimensions in our simulation studies. After the above 3D processes, the image reconstruction can be performed slice-by-slice for the VVF collimation geometry in two dimensions, as shown below.

2.4 Reconstruction with Non-uniform Attenuation Compensation for VFF Collimators

For both the treatment of Poisson noise and the compensation for scatter and DDRV, all the procedures are performed in 3D domain. For attenuation compensation with VFF collimators [28][31][32][33][34][35], we can process it in a 2D manner slice-by-slice, since the photon absorption effect in the VFF collimation is a 2D problem. Based on the Novikov's parallel-beam non-uniform attenuation reconstruction formula, we derived two different variable fan-beam reconstruction algorithms: one is the approximated algorithm [25]; and the other is the ray driven exact algorithm [27]. When focal length is long enough, the approximate method can obtain good result and run very fast. Exact method is ray-driven, that means it reconstructs image ray-by-ray. This would cost more computing time, but the speed can be improved with pre-process storage of some parameters, instead of computing them on the flight.

2.4.1 Approximated reconstruction algorithm

Any ray (p, β) in the VFF geometry can be seen as a ray (x_r, ϕ) in the parallel-beam geometry. Let $D(p)$ be the focus length at bin position *p*. The relation between these two geometries is:

$$\begin{aligned} \phi &= \beta + \gamma = \beta + tg^{-1}\frac{p}{D(p)} \\ x_r &= p\cos\gamma = \frac{pD(p)}{\sqrt{D^2(p) + p^2}}. \end{aligned} \tag{12}$$

For VFF geometry, we have

$$\begin{aligned} (Hg)(x_r) &= \frac{1}{\pi}\int \frac{g(x_r^{"})}{x_r - x_r^{"}} dx_r^{"} \\ &= \frac{1}{\pi}\int \frac{g(p^{"})}{(p - p^{"})\frac{UD(p^{"})}{\sqrt{D^2(p^{"}) + p^{"2}}}} d\left(\frac{p^{"}D(p^{"})}{\sqrt{D^2(p^{"}) + p^{"2}}}\right) \end{aligned}$$

$$= \frac{1}{\pi}\int \frac{g(p")}{(p-p")}\cdot\left(\frac{\sqrt{D^2(p")+p"^2}}{UD(p")}\right)\cdot\frac{D^3(p")+p"^3D'(p")}{\left(\sqrt{D^2(p")+p"^2}\right)^3}dp"$$

$$= \frac{1}{\pi}\int \frac{g(p")}{p-p"}\cdot\frac{D^2(p")}{U(D^2(p")+p"^2)}\left(1+p"^3D'(p")/D^3(p")\right)dp" = (Hg^e)(p) \tag{13}$$

where

$$g^e(p) = g(p)\cdot\frac{D^2(p)}{U(D^2(p)+p^2)}\left(1+p^3D'(p)/D^3(p)\right). \tag{14}$$

The approximated reconstruction formula for VFF collimator geometry of non-uniform attenuation is represented by the following equations

$$f(x,y) = \frac{1}{4\pi}[\frac{\partial}{\partial x}Bc(x,y)+\frac{\partial}{\partial y}Bs(x,y)]$$

$$Bc(x,y) = \frac{1}{4\pi}\int_0^{2\pi}[e^{(D_\phi a_\phi)(x_r,y_r)}ga_\phi{}'(x_r)]\cos\phi\, d\phi$$

$$Bs(x,y) = \frac{1}{4\pi}\int_0^{2\pi}[e^{(D_\phi a_\phi)(x_r,y_r)}ga_\phi{}'(x_r)]\sin\phi\, d\phi \tag{15}$$

where

$$\begin{aligned} ga_\phi{}'(x_r) = e^{-A_\beta(p)}&[\cos(C_\beta(p))H\left(\cos(C_\beta(p))e^{A_\beta(p)}g_\beta(p)W(p)\right)\\ &+\sin(C_\beta(p))H\left(\sin(C_\beta(p))e^{A_\beta(p)}g_\beta(p)W(p)\right)] \end{aligned} \tag{16}$$

$$A_\beta(p) = \frac{1}{2}Ra_\beta(p),\ C_\beta(p) = H(A_\beta(p)W(p)),$$

$$W(p) = \frac{D^2(p)}{U(D^2(p)+p^2)}\left(1+p^3D'(p)/D^3(p)\right). \tag{17}$$

Notations $f(x)$ and $a(x)$ were defined before for the activity phantom to be reconstructed and the attenuation coefficient across the body, respectively. Notation $g_\phi(x_r)$ is the projection datum at position x_r with projection angle ϕ, H denotes for the Hilbert transform and R represents the Radon transform.

When $D(p) = a + k\,|\,p\,|$, we have $D'(p) = ksign(p)$. For a point (r,θ), its projection on the detector is $\hat{p}$

$$\hat{p} = \frac{-b+\sqrt{b^2+4kar\,|\cos(\beta-\phi)|}}{2ksign[\cos(\beta-\phi)]}. \tag{18}$$

2.4.2 Exact reconstruction algorithm

For each ray (p,β), we can build a local coordinate system (u,v). The relation between this local coordinate system and the original coordinate system is:

$$\begin{aligned} u &= x\cos\phi + y\sin\phi\\ v &= -x\sin\phi + y\cos\phi \end{aligned}. \tag{19}$$

Our ray-driven exact VFF reconstruction formula can be written as

$$f(x,y) = \frac{1}{4\pi}(\frac{\partial}{\partial x}B_C(x,y)+\frac{\partial}{\partial y}B_S(x,y))$$

$$B_C(x,y) = \int_0^{2\pi}\int_{-\infty}^{\infty}[e^{(D_\phi a_\phi)(u,v)}ga_{(\beta,p)}(u)]\cos\phi\,|\,J\,|dpd\beta$$

$$B_S(x,y) = \int_0^{2\pi}\int_{-\infty}^{\infty}[e^{(D_\phi a_\phi)(u,v)}ga_{(\beta,p)}(u)]\sin\phi\,|\,J\,|dpd\beta \tag{20}$$

where

$$ga_{(\beta,p)}(u) = e^{-A_\phi(u)}[\cos(E_\phi(u))H\left(\cos(E_\phi(x_r))e^{A_\phi(x_r)}g(p,\beta)\delta(u-x_r)\right)+\sin(E_\phi(u))H\left(\sin(E_\phi(x_r))e^{A_\phi(x_r)}g(p,\beta)\delta(u-x_r)\right)]$$

$$E_\phi(u) = HA_\phi(u), \quad \text{and} \quad A_\phi(u) = \frac{1}{2}Ra_\phi(u) \tag{21}$$

the Jacobian $|J|$ is given by

$$|J| = \begin{vmatrix} \partial x_r/\partial p & \partial x_r/\partial\beta \\ \partial\phi/\partial p & \partial\phi/\partial\beta \end{vmatrix} = \frac{D^3(p)+p^3D'(p)}{\sqrt{(D^2(p)+p^2)^3}}. \tag{22}$$

where H and R have been defined before. The relation between (x,y) and (u,v) is shown by equation (19). The relation between (p,β) and (x_r,ϕ) is shown by equation (12). Therefore, (u,v) can be obtained by (x,y), and (x_r,ϕ) can be obtained by (p,β).

3. SIMULATIONS

Figure 2 shows the reconstructed images using our approximated and exact variable fan-beam non-uniform attenuation reconstruction algorithm. Projection data of 128 bins and 128 stops evenly distributed over 360 degrees were simulated from the Shepp-Logan mathematical phantom [21] with non-uniform attenuation on an image array of 128x128 size, see Figure 2.

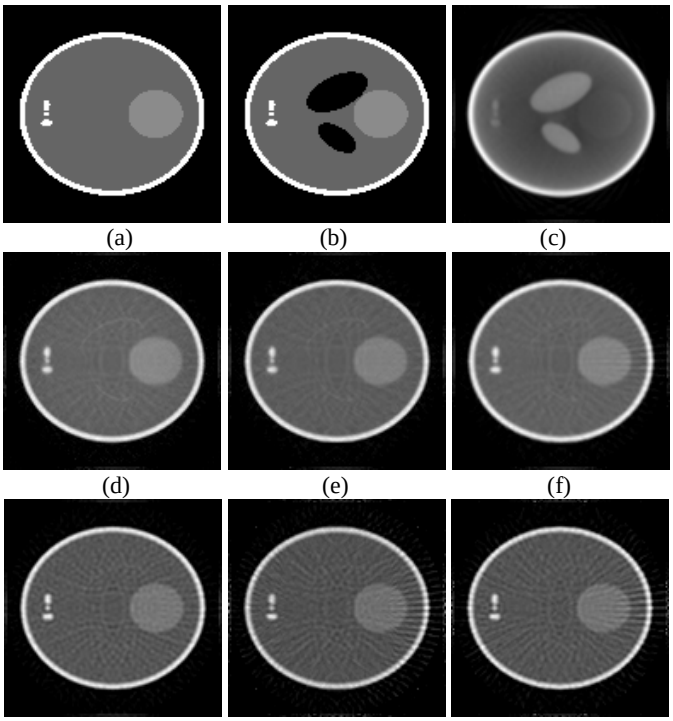

Figure 2: Reconstruction results using our methods. D(p) is focus length in pixel units, image size is 128×128. (a) Activity Phantom. (b) Attenuation Map. (c) Reconstruction without attenuation compensation. (d) Fan-beam D(p) = 300. (e) Fan beam D(p) = 1000. (f) VFF D(p)=300+30|p|. Images of (d)-(e)-(f) are the reconstruction results using our approximated method. (g) Parallel-beam D(p) = ∞. (h) Fan beam D(p) = 300. (i) VFF D(p) = 300+30|p|. Images of (g)-(h)-(i) are the reconstruction results using our ray-driven exact method.

On the top right or Figure 2(c), a reconstruction of variable fan-beam collimated projection data is shown without attenuation compensation. A strong effect of non-uniform attenuation is seen. In Figure 2, images of (d), (e) and (f)

are reconstruction results using our approximated method. With fan-beam collimators of focal lengths of 300 and 1000 pixel units, i.e., a short and long focal lengths, we obtained almost identical results to the original image, see images of (d) and (e) in Figure 2. By the variable focal-length function of $D(p)=300+30|p|$, the reconstructed result, see Figure 2(f), was almost identical to those of the fan-beam reconstructions. In Figure 2, images of (g), (h) and (i) are reconstruction results using our ray-driven exact method. For fan-beam geometry, the focal length was chosen as $D(p) = 300$ in pixel units. For VFF geometry, we tested two focal length functions of $D(p) = 200+10|p|$ and $D(p) = 300+30|p|$. We obtained almost identical results to the original image.

To evaluate the performance of our proposed analytical reconstruction scheme, Monte Carlo simulations (SIMIND, Ljungberg, e*t al*. 1994) were used to generate realistic projection data from the MCAT digital torso phantom with defects inside myocardium. The phantom was scanned by a SPECT system with high-resolution, VFF collimators and triple-energy-window acquisitions. Projection data of 128 bins and 128 stops evenly distributed over 360 degrees were sampled with non-uniform attenuation. The preliminary simulation results showed that reconstruction results become better and better after noise reduction, scatter removal, DDRV correction and attenuation compensation (see Figure 3).

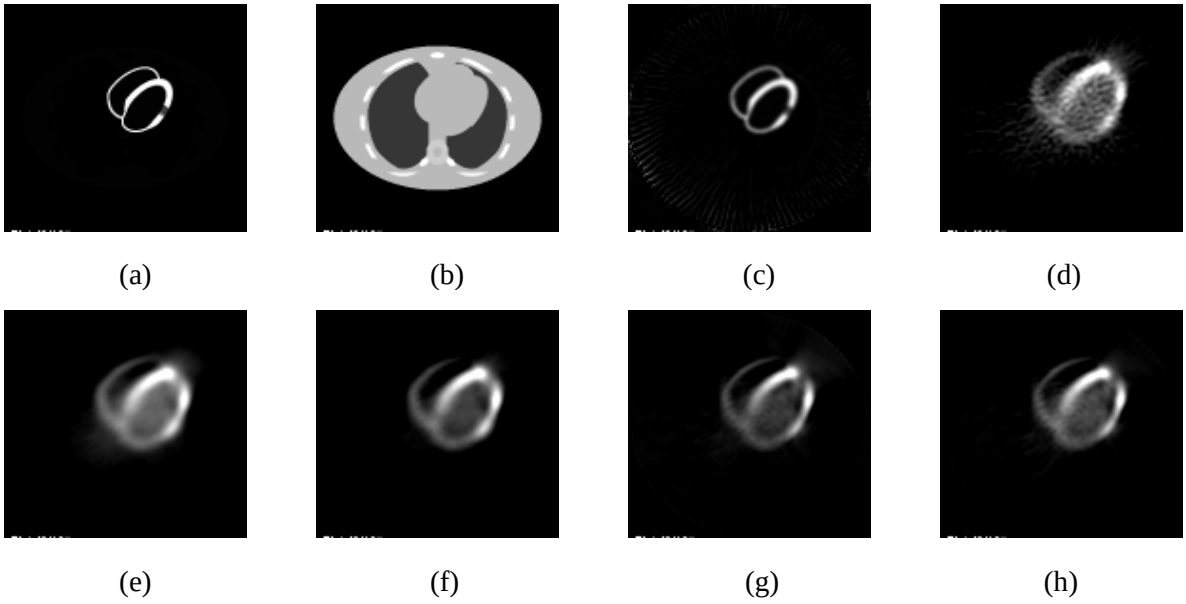

Figure 3: MCAT phantom and reconstructed images from Monte Carlo simulation: (a) activity phantom; (b) attenuation map; (c) attenuation reconstruction from noise-free projection data (demonstrating correct implementation); (d) FBP reconstruction directly from noisy projection data; (e) FBP reconstruction after noise reduction; (f) FBP reconstruction after noise smoothing and scatter removal; (g) FBP reconstruction after noise reduction, scatter removal, and DDRV correction; (h) reconstruction of the proposed analytical scheme after attenuation compensation, DDRV correction, scatter removal and noise reduction. (Variable focal length function is $D(p)=174.5000+0.1001\ p^2$).

4. CONCLUSION

In this paper, we described an analytical VFF reconstruction scheme that provides a simultaneous compensation for non-uniform attenuation, object-specific scatter, and system-dependent DDRV, as well as an accurate treatment of the non-stationary, signal-dependent Poisson noise. Simulation results show that our analytical variable focal-length fan-beam reconstruction for quantitative SPECT with simultaneous compensation for all these degradations is feasible. For clinical application, we will need more validations for the whole scheme using both the Monte Carlo simulation and the experimental phantom studies, and finally utilizing the real patient data.

REFERENCES

[1] FJ. Anscombe, "The transformation of Poisson, binomial and negative-binomial data", *Biometrics*, **35**: 246-254,1948.

[2] E. V. Arbuzov, A. L. Bukhgeim, and S. G. Kazantsev, "Two-dimensional tomography problems and the theory of A-analytic functions", *Siberian Advances in Mathematics*, **8**(4): 1-20, 1998.

[3] MH. Bourguignon, M. Wartski, N. Amokrane *et al*, "Le spectre du rayonnement diffusé dans la fenétre du photopic: analyse et proposition d'une methode de correction", *Médecine Nucléaire*, **17**:53-58, 1993

[4] L. Van. Elmbt and S. Walrand, "Simultaneous correction of attenuation and distance-dependent resolution in SPECT: an analytical approach", *Phys. Med. Biol*. **38**:1207-1217, 1993.

[5] A. R. Formiconi, A. Pupi, and A. Passeri, "Compensation of spatial system response in SPECT with conjugate gradient reconstruction technique", *Phys. Med. Biology*, **34**: 69-84, 1990.

[6] S. J. Glick, B. C. Penney, M. A. King, and C. L. Byrne, "Noniterative compensation for the distance-dependent detector response and photon attenuation in SPECT imaging", *IEEE Trans. Med. Imaging*, **13**: 363-374, 1994.

[7] G. T. Gullberg, *The Attenuated Radon Transform: Theory and application in medicine and biology*, Ph.D. Dissertation, University of California at Berkeley, CA, 1979.

[8] G. Han, *Image Reconstruction in Quantitative Cardiac SPECT with Varying Focal-length Fan-beam Collimators*, Ph.D. Dissertation, State University of New York at Stony Brook, NY, 2000.

[9] BR. Hunt and O. Kübler, "Karhunen-Loeve multi-spectral image restoration, part I: theory", IEEE *Trans. Acoustics, Speech, and Signal Processing*, **ASSP-32**: 592-600, 1984.

[10] L. Kunyansky, "A new SPECT reconstruction algorithm based on the Novikov's explicit inversion formula", *Inverse Problems*, **17**: 293-306, 2001.

[11] R. M. Lewitt, P. R. Edholm, and W. Xia, "Fourier method for correction of depth-dependent blurring", *SPIE Medical Imaging III*, **1092**: 232-239, 1989.

[12] T. Li, J. Wen, and Z. Liang, "Compensation for non-stationary detector response in analytical varying focal-length fan-beam SPECT reconstruction", *IEEE NSS-MIC Conf Record*, in CD-ROM, 2002.

[13] X. Li, G. Han, H. Lu, L. Li, and Z. Liang, "A new scatter estimation method using triple window acquisition to fit energy spectrum," *The 48th Annual Meeting of the Society of Nuclear Medicine, JNM*, **42**: 194, 2001.

[14] Z. Liang, J. Ye, J. Cheng, and D. Harrington, "Quantitative brain SPECT in three dimensions: an analytical approach to non-uniform attenuation without transmission scans", in *Computational Imaging and Vision book series*, by Kluwer Academic Publishers, pp. 117-132, 1996.

[15] Z. Liang, T. G. Turkington, D. R. Gilland, R. J. Jaszczak, and R. E. Coleman, "Simultaneous compensation for attenuation, scatter, and detector response of SPECT reconstruction in three dimensions", *Phys. Med. Biology*, **37**: 587-603, 1992.

[16] H. Lu, D. Chen, L. Li, and *et al*, "A combined transformation of ordering SPECT sinograms for signal extraction from measurements of Poisson noise", *SPIE Medical Imaging*, 4322: 943-951:2001.

[17] H. Lu, J. Wen, X. Li, T. Li, G. Han, and Z. Liang, "Towards analytical solution for 3D SPECT reconstruction with non-uniform attenuation and distance-dependent resolution variation: a Monte Carlo simulation study," *SPIE Medical Imaging*, **4684**: 20-28. 2002

[18] F. Natterer, "Inversion of the attenuated Radon transform", *Inverse Problems*, **17**: 113-119, 2001.

[19] R. Novikov, "An inversion formula for the attenuated X-ray transformation", Preprint, May 2000.

[20] K. Ogawa, Y. Harata, T. Ichihara, A. Kubo, and S.Hashimoto, "A practical method for position dependent Compton scatter correction in SPECT ", *IEEE Trans. Med. Imaging*, **10**: 408-412, 1991.

[21] L. Shepp and B. Logan, "The Fourier reconstruction of a head section", *IEEE Trans. Nucl. Science*, **21**: 21-43, 1974.

[22] B. M. W. Tsui, H. B. Hu, D. R. Gilland, and G. T. Gullberg, "Implementation of simultaneous attenuation and detector response correction in SPECT", *IEEE Trans. Nucl. Science*, **35**: 778-783, 1988.

[23] B. M. W. Tsui and G. T. Gullberg, "The geometric transfer function for cone and fan beam collimators", *Phys. Med. Biology*, **35**: 81-93, 1990.

[24] O. J. Tretiak and C. E. Meta, "The exponential Radon transform", *SIAM J. Appl. Math*, **39**: 341-354, 1980.

[25] J. Wen, T. Li, X. Li, and Z. Liang, "Fan-beam and variable-focal-length fan-beam SPECT reconstruction with non-uniform attenuation", *J. Nuclear Medicine Technology*, **30**: 97, 2002.

[26] J. Wen, T. Li, and Z. Liang, "Ray-driven analytical fan-beam SPECT reconstruction with non-uniform attenuation", *Proc. IEEE Intl. Sym. on Biomedical Imaging*, pp. 629-632, 2002.

[27] J. Wen, T. Li and J. Liang, "A ray-driven approach to analytical SPECT reconstruction of non-uniform attenuation with variable focal-length fan-beam collimators", *IEEE NSS-MIC Conf Record*, in CD-ROM, 2002.

[28] Y. Weng, L. Zeng, and G. T. Gullberg, "Analytical inversion formula for uniformly attenuated fan-beam projections", *IEEE Trans. Nucl. Science*, **44**: 243-249, 1997.

[29] W. Xia, R. M. Lewitt, and P. R. Edholm, "Fourier correction for spatially variant collimator blurring in SPECT", *IEEE Trans. Med. Imaging*, **14**: 100-115, 1995.

[30] J. Ye and Z. Liang, "Depth-dependent resolution deconvolution for myocardial perfusion SPECT with non-circular scan orbit", *J. Nuclear Medicine*, **35**: 190, 1994.

[31] J. You, S. Bao, and Z. Liang, "Benefits of angular expression to reconstruction algorithms for collimators with spatially varying focal length", *IEEE Trans. Med. Imaging*, **16**: 527-531, 1997.
[32] J. You, Z. Liang, and S. Bao, "A harmonic decomposition reconstruction algorithm for spatially varying focal length collimators", *IEEE Trans. Med. Imaging*, **17**(6): 995-1002, 1998.
[33] J. You, Z. Liang, and G. L. Zeng, "A unified reconstruction framework for both parallel-beam and variable focal-length fan-beam collimators by a Cormack-type inversion of exponential Radon transform", *IEEE Trans. Med. Imaging*, **18**(1): 59-65, 1999.
[34] G. L. Zeng, G. T. Gullberg, R. J. Jaszczak, and J. Li, "Fan-beam reconstruction algorithm for a spatially varying focal length collimator", *IEEE Trans. Med. Imaging*, **12**(3): 575-582, 1993.
[35] G. L. Zeng and G. T. Gullberg, "A backprojection filtering algorithm for a spatially varying focal length collimator", *IEEE Trans. Med. Imaging*, **13**(3): 549-556, 1994.
[36] G. L. Zeng, G. T. Gullberg, B. M. W. Tsui, and J. A. Terry, "Three-dimensional Iterative Reconstruction Algorithm with Attenuation and Geometric Point Response Correction", *IEEE Trans. Nucl. Science*, **38**: 693-702, 1991.
[37] G. L. Zeng and G. T. Gullberg, "Frequency domain implementation of the three-dimensional geometric point response correction in SPECT imaging", *IEEE Trans. Nucl. Science*, **39**: 1444-1453, 1992.